DAYTIME TURBULENCE STATISTICS ABOVE A STEEP FORESTED SLOPE

E. VAN GORSEL, A. CHRISTEN, C. FEIGENWINTER, E. PARLOW and R. VOGT
Institute of Meteorology, Climatology and Remote Sensing, University of Basel, Basel, Switzerland

(Received in final form: 30 December 2002)

Abstract. Six levels of simultaneously sampled ultrasonic data are used to analyse the turbulence structure within a mixed forest of 13 m height on a steep slope (35°) in an alpine valley. The data set is compared to other studies carried out over forests in more ideal, flat terrain. The analysis is carried out for 30-min mean data, joint probability distributions, length scales and spectral characteristics.

Thermally induced upslope winds and cold air drainage lead to a wind speed maximum within the trunk space. Slope winds are superimposed on valley winds and the valley-wind component becomes stronger with increasing height. Slope and valley winds are thus interacting on different spatial and time scales leading to a quite complex pattern in momentum transport that differs significantly from surface-layer characteristics. Directional shear causes lateral momentum transports that are in the same order or even larger than the longitudinal ones. In the canopy, however, a sharp attenuation of turbulence is observed. Skewed distributions of velocity components indicate that intermittent turbulent transport plays an important role in the energy distribution.

Even though large-scale pressure fields lead to characteristic features in the turbulent structure that are superimposed on the canopy flow, it is found that many statistical properties typical of both mixing layers and canopy flow are observed in the data set.

Keywords: Complex terrain, Forest, Mixing layer analogy, Spectra, Turbulence structure.

1. Introduction

Topography strongly modifies the exchange of energy and momentum between the Earth's surface and adjacent atmosphere. Modifications occur through a wide range of processes including radiative, thermodynamic and several dynamic flow effects (Raupach and Finnigan, 1997). Topography can lead to mechanical blocking or channelling of the flow, and, apart from dynamic effects, topography determines the temporal and spatial distribution of radiation (Whiteman and Allwine, 1989). Different inclination and azimuth angles of surfaces lead to highly variable energy input, and radiative heating or cooling causes thermally induced circulations. While in mountainous terrain the mean wind field with local thermally induced circulation patterns is fairly well understood (e.g., Barry, 1992; Egger, 1990; Whiteman, 1990), there remains a lack of knowledge regarding turbulent exchange processes in mountainous regions (Rotach et al., 2000), and studies of turbulence in complex terrain have mainly been restricted to hills so far (Wood, 2000).

Boundary-Layer Meteorology **109:** 311–329, 2003.

In addition to topography roughness elements contribute to the complexity of the flow. For example momentum is absorbed through the depth of a plant canopy by aerodynamic drag on the plants. As a large fraction of the Swiss southern Alps is forested this study concentrates on the analysis of observations made at a steep forested slope. During the last few decades many investigations have been carried out in order to improve knowledge of turbulence structure in and above plant canopies; they range from model canopies to horizontally homogeneous, flat forests. Such studies have led to a general view of canopy turbulence that is now widely accepted, and can be depicted as a 'family portrait' of the different experiments (Kaimal and Finnigan, 1994; Raupach et al., 1996; Raupach and Thom, 1981). Reviews on turbulence in plant canopies have recently been given in Finnigan (2000) and Finnigan and Brunet (1995). The most important features that distinguish canopy from surface-layer turbulence can be summarised as follows: (i) The wind profile has an inflection point at the canopy top that is established by drag in the canopy. The inflection leads to an instability that controls the turbulence structure in the canopy and leads to statistics that are related closer to mixing than to surface-layer turbulence; (ii) second-order moments decrease with height; (iii) skewnesses in the canopy are large and the canopy turbulence is dominated by large coherent structures.

It must be expected that topographic features such as found in the Riviera Valley in Switzerland strongly influence the turbulence structure. Due to a lack of existing theories to describe turbulence in such a complex environment we compare the experimental data with the 'family portrait'. This gives an impression on how dominantly the plant canopy is responsible for the turbulence structure and how it is modified by topography. We here concentrate on the mean daily circulation patterns and the associated momentum transport, and compare single point statistics, joint probability distributions and spectral properties with results obtained in studies treating canopy turbulence in flat terrain. We focus on a period where thermally driven forcing is strong and well-developed slope and valley wind systems can be expected. Therefore a period (September 7 to 15) is selected that was characterized by an extensive anticyclone over north-east Europe with synoptic winds from the north–east, changing to weak winds from the south–west at the end of the period.

2. Site Description and Measurements

The measurement campaign was carried out during the MAP-RIVIERA project, which lasted from July to October 1999. A detailed description of the experiment is given in Rotach et al. (2000). The Riviera valley is situated in the Swiss southern Alps, and is oriented roughly north-north-west to south-south-east and ranges from about 250 m a.s.l at the valley floor to 2500 m a.s.l on both sides (Figure 1). The valley is 1.5 km wide at the valley floor and eastern and western slopes are inclined at angles of 30° and 35° respectively.

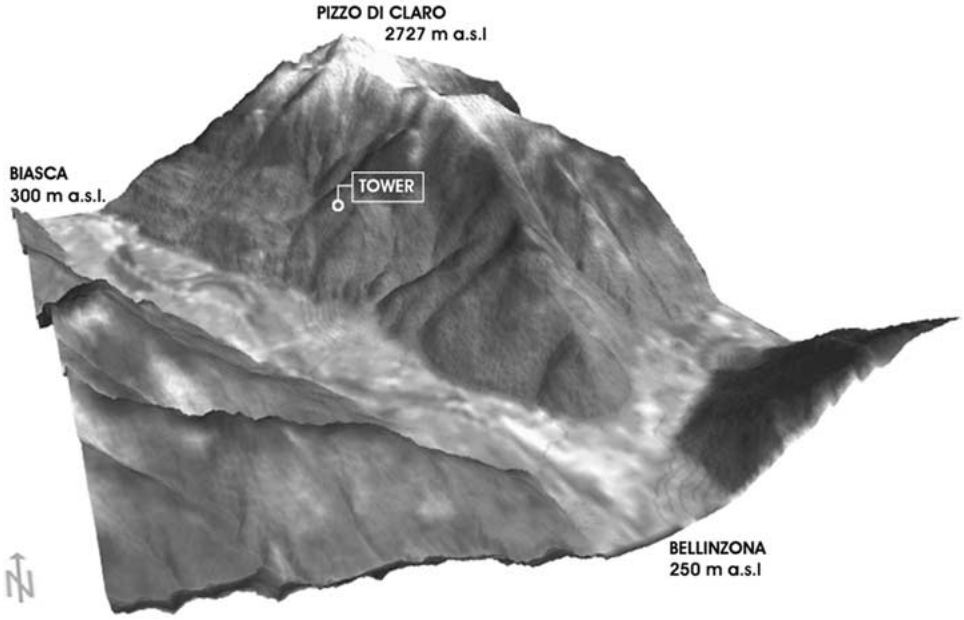

Figure 1. Topographical map based on the digital elevation model of the Riviera valley.

Here we report measurements carried out in and above a mixed forest (46°16′14″ N, 9°02′11″ E, 1030 m a.s.l.). The slope was inclined at an angle of 35° and exposed to the west–south–west. The forest mainly consisted of birch trees, other species being chestnut, beech and hazel. The mean tree height h was 13 m and the leaf area index about 4; the forest floor was covered with sparse understorey vegetation with heights up to 0.4 m. The tower was mounted in the middle of a relatively 'homogeneous' part of the slope. Uphill and downhill, the fetch was around 150 to 200 m with similar homogeneous surface conditions, both in terms of tree height and species, prevailing 100 m slope parallel northwards and southwards (Figure 2).

At the top of a 22 m high tower all components of the radiation balance were measured with a CNR1 radiometer (Kipp and Zonen; Delft, The Netherlands). The radiometer as well as six ultrasonic anemometer thermometers (sonics) were installed slope parallel, the former in order to measure the radiation balance relevant to the slope (Whiteman and Allwine, 1989), the latter in order to minimise flow distortion effects (Christen et al., 2001). The sonics were mounted slope parallel at 2 m distance from the triangular lattice tower of 0.6 m side length. All sonic raw data were stored synchronously on an industrial personal computer for further analysis.

Preceding the MAP-RIVIERA experiment a wind-tunnel study was carried out in order to test instrument responses for several angles of attack of the flow

TABLE I

Overview of sonic types and measurements. The output variables u, v, w represent the wind velocity components and θ_{sv} the sonic temperature; z is the measuring and h the canopy height.

Notation	z/h	Instrument type	Internal sampling rate (Hz)	Output sampling rate (Hz)	Output variables	Calibration
	1.74	Gill HS[1]	100	20	u, v, w, θ_{sv}	Matrix
	1.29	Gill R2[1]	166.6	20.83	Transit counts	Matrix
Upper canopy	0.99	Gill R2[1]	166.6	20.83	Transit counts	Gill
Lower canopy	0.72	Gill R2[1]	166.6	20.83	Transit counts	Gill
Upper trunk space	0.49	CSAT3[2]	60	20	u, v, w, θ_v	Matrix
Lower trunk space	0.14	CSAT3[2]	60	20	u, v, w, θ_v	Matrix

[1] Gill Instruments Ltd. U.K.
[2] Campbell Scientific Inc. U.S.A.

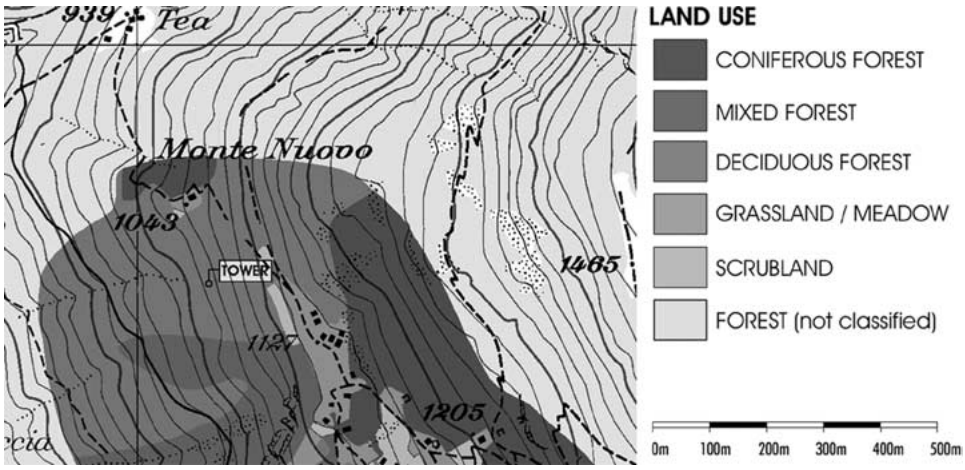

Figure 2. Land use map of surrounding of tower. Base Map: Carta Nazionale della Svizzera 1314 1:25′000, 1998, © Bundesamt für Landestopographie 2000 (JD002102).

and to create a calibration matrix for the sonics (Vogt, 1995). A subsequent field intercomparison of the sonics took place under near ideal conditions in order to test calibrations under 'real flow' conditions and to obtain information about differences between the sensors and sensor types (Christen et al., 2000).

3. Data Handling and Methods

Data analysis is based on 30-min periods. In the following, mean data are denoted by an overbar ($\bar{x}$) and fluctuations by a prime (x'), where x represents any variable. For each time period and each height data are rotated into a right-handed Cartesian coordinate system with the x-axis aligned to the mean wind ($\bar{u}$) such that the mean lateral and vertical wind velocity components ($\bar{v}$, $\bar{w}$) are zero. Averages and higher order moments are calculated by applying Reynolds averaging and linear detrending (Rannik and Vesala, 1999).

An estimate of the joint probability distribution of horizontal and vertical fluctuations normalised by their respective standard deviations (u'/σ_u, v'/σ_v, w'/σ_w) is calculated by counting the number of occurrences of pairs in the same class, where the 20 times 20 classes are spaced equally between ± 2 normalised standard deviations. The result is then divided by the total number of data points leading to a probability in the range of [0, 1]. The result indicates whether there exists any dominance of fast or slow, upward or downward movements.

Information on the size of eddies dominant in the flow can be gained in several ways. The distribution of average eddy size through the whole canopy has been

investigated by calculating the integral length scales $L_{u,v,w}$. They are derived from the autocorrelation function

$$L_x = \frac{\bar{u}}{\sigma_x^2} \int_0^\infty \overline{x'(t)x'(t+\xi)} d\xi,$$

where x represents any velocity component and ξ is the time lag. In practice, the integration has been carried out up to the first zero crossing in the autocorrelation function (Kaimal and Finnigan, 1994). Another way to assess dominant length scales is to look at the maximum peak frequency $f_{\max}$ of power spectra, and for this purpose Fourier spectra have been calculated. In order to avoid broadening of the spectra cosine tapering has been applied to the rotated and detrended data before calculating the fast Fourier transforms. Raw spectral estimates were then averaged into 60 logarithmically spaced frequency bands. For calculating mean spectra normalised single spectra were interpolated with a cubic spline and the fitted curves where then averaged into logarithmically spaced classes.

For most analysis data were pooled into three stability classes. The stability classes were taken from the uppermost level. In order to avoid runs measured at night with neutral to unstable stability conditions, stability classes were modified depending on daytime (see also Figure 3). Stability classes used in this article are defined as follows: neutral (evening transition ETR: $0.05 \geq h/L \geq -0.05$), weakly unstable (daytime DT: $-0.05 > h/L > -0.5$) and unstable (morning transition MTR: $-0.5 \geq h/L$), where L is the Obukhov length, calculated as $L = -u_*^3/(k(g/\theta)\overline{w'\theta_v'})$, where k the von Karman constant is taken as 0.4 and g is the acceleration due to gravity (9.8 m s^{-2}). The friction velocity u_* is always calculated as $u_* = (\overline{u'w'}^2 + \overline{v'w'}^2)^{1/4}$.

4. Results

4.1. Diurnal patterns

Figure 3a shows the diurnal course of net radiation measured above the canopy. Clear sky conditions prevailed during the selected measuring period with the exception of September 11, which was slightly overcast. As stability has a crucial influence on turbulent exchange processes an overview of the distribution of stability classes is given in Figure 3h. Stability classes show a quite regular pattern: During daytime from around 1200 to 1800 CET a good coupling exists through the canopy. The conditions in and above the canopy are mainly unstable to weakly unstable. In the evening the atmospheric conditions typically change from neutral to weakly stable in the crown space and above, while stability conditions in the trunk space are variable. During the night stability conditions are highly variable at all levels except the lowest, where instability dominates. The regime in the lower

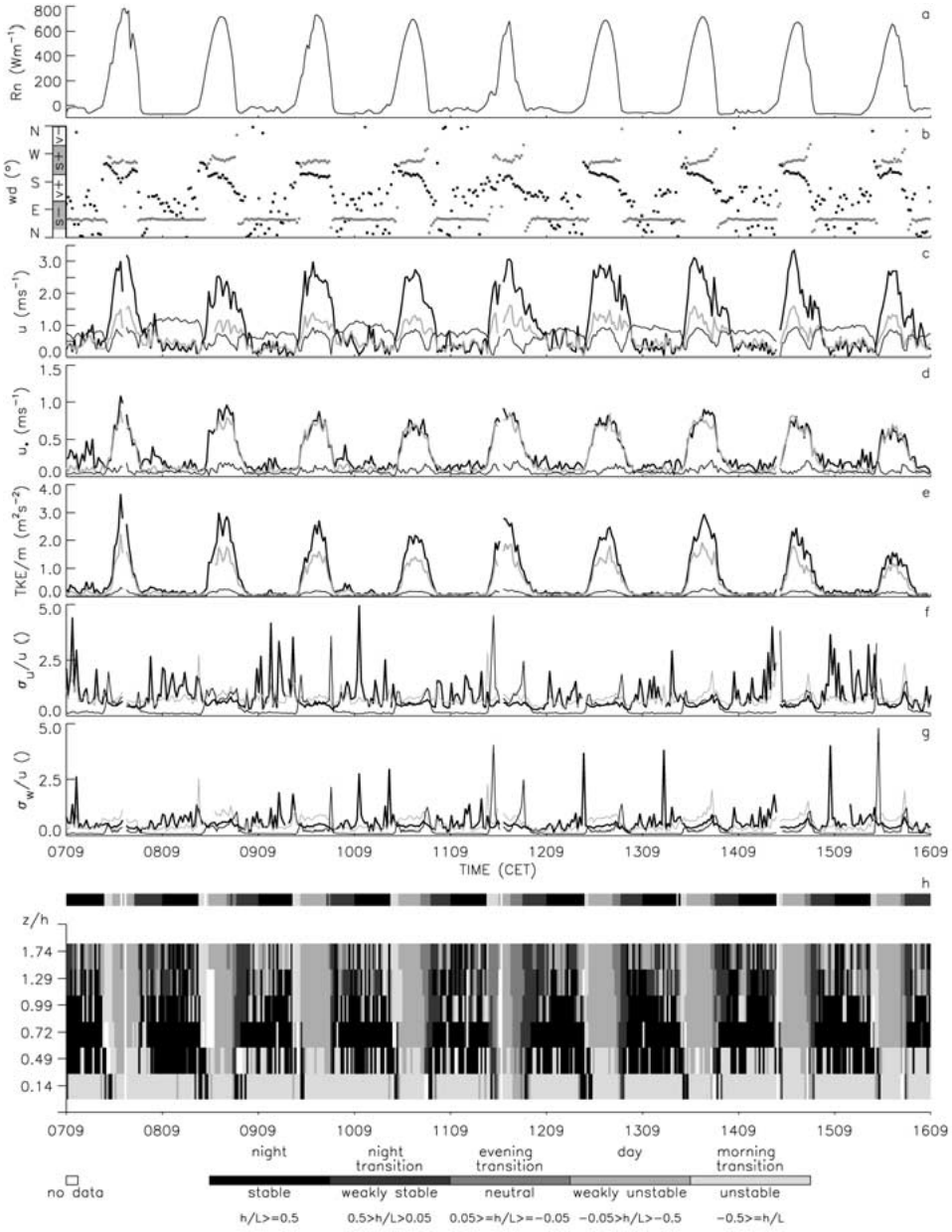

Figure 3. Diurnal patterns of (a) net radiation (b) wind direction (c) wind speed (d) friction velocity (e) turbulent kinetic energy per unit mass (f), (g) turbulence intensity of the longitudinal and vertical wind component respectively and (h) the stability conditions at all measurement heights. Additionally the stability index is indicated. Symbols are used as follows: Thin black lines stand for measurements at $z/h = 0.14$, grey lines for measurements at $z/h = 0.99$, and black thick lines for measurements at $z/h = 1.74$. In Figure 1b v stands for valley and s for slope, $+$ and $-$ indicate upward and downward respectively; the grey symbols stand for measurements at $z/h = 0.14$ and black symbols for measurements at $z/h = 1.74$.

canopy is mainly very stable. In the late morning, finally, there is a short period where unstable values can be observed in the crown space and above.

Due to the anticyclonic forced weather conditions pronounced slope and valley wind systems developed. Both wind systems develop due to horizontal pressure gradients that are built up hydrostatically by the changing low-level horizontal temperature gradients (Whiteman, 1990). The superposition of the two systems is shown in Figure 3b. One clearly sees that in the lower trunk space wind directions have almost a bimodal distribution. In the morning hours around 0900 CET the wind direction switches from downslope to upslope in connection with the changing sign of the radiation balance. In the evening the wind rotates clockwise back to a downslope direction. After having evolved the upslope and downslope winds are very persistent. This simple pattern is not found above the canopy where only in the morning transition hours upslope winds are observed. Later on in the day the upslope winds are superimposed upon an upvalley component, which becomes increasingly stronger. In the evening the wind direction often turns continuously in a counterclockwise sense to a north-easterly direction, which then shows large variability during the night.

Vector average wind speeds $\bar{u}$ at $z/h = 1.74$ and at $z/h = 0.99$ show a similar pattern of temporal variation (Figure 3c). During the day $\bar{u}$ decreases strongly with height but has a secondary maximum in the upper trunk space (not shown). During the night, maximum wind speed is reached at the lowest level where cold air drainage is most effective. (The diurnal patterns of the components of the wind velocity will be described in the following section in more detail.) The local friction velocity u_* is very similar at canopy top and above but decreases rapidly in the canopy (Figure 3d). Even though during the night $\bar{u}$ is strongest at $z/h = 0.14$, the friction velocity, the turbulent kinetic energy per unit mass (TKE/m) and the turbulent intensities are very small (Figures 3e–g). This indicates a very persistent cold air drainage. Even the large changes in turbulence intensities above the canopy do not result in corresponding variations in the trunk space where the flow is decoupled from the flow above.

Figure 4a shows the mean diurnal pattern of the slope and valley wind components. At the topmost level, upslope winds are evolving when the radiation balance becomes positive. With decreasing height the switch to upslope flow increasingly lags behind the topmost level and about 1.5 hr later upslope winds are observed at the lowest level too. In the fully developed upslope wind system a secondary maximum of wind speed is observed in the trunk space and minimum values are found in the crown space. This is contrary to the valley wind component, which decreases continuously with decreasing height and does not penetrate down into the trunk space. The valley wind system evolves shortly after the slope wind system, but decays several hours later. The delay in the evening transition between the top and the lowest level for the slope component is only about half as long (40 min) as that in the morning. During the night a maximum cold air drainage flow is located in the lower trunk space. In the canopy wind speed is reduced and a secondary

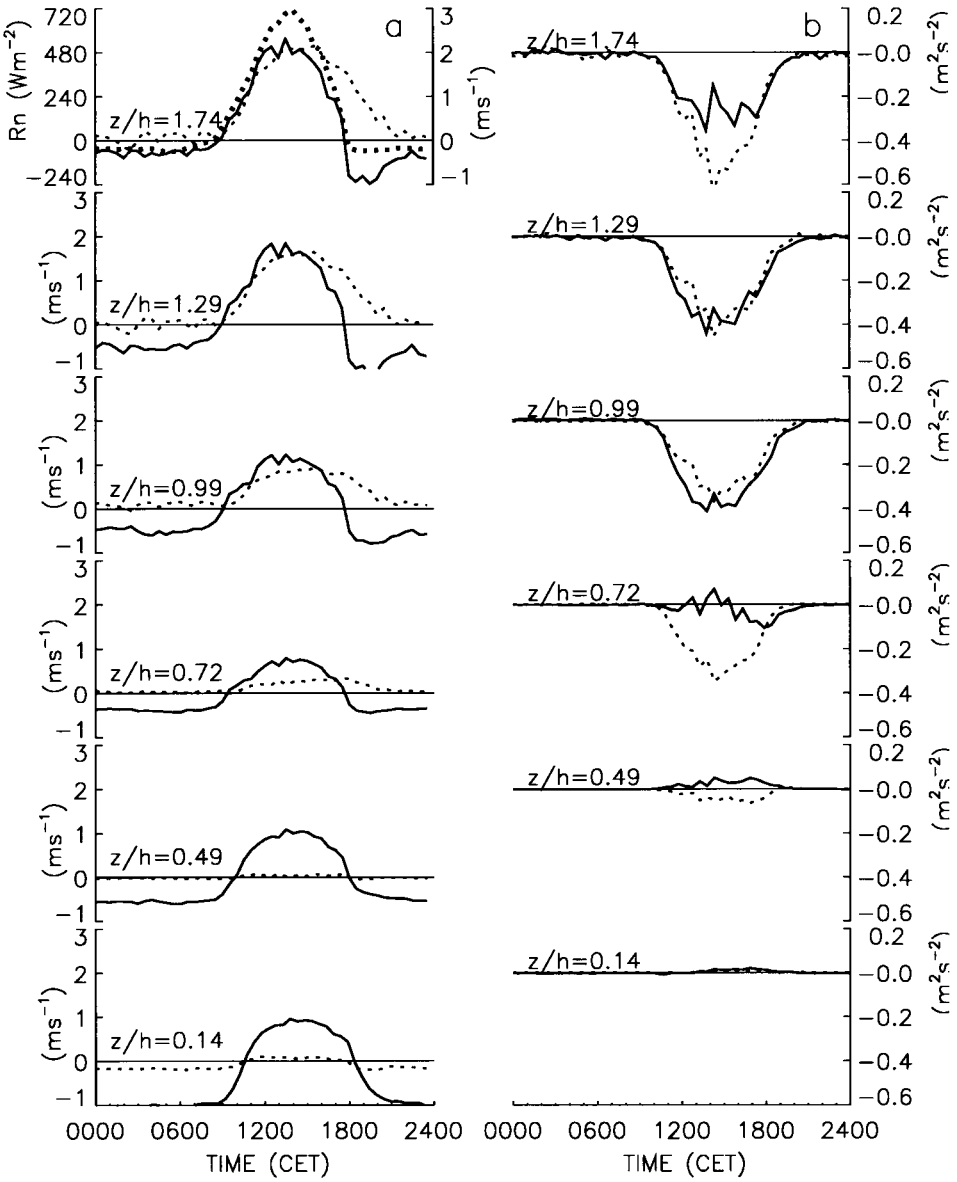

Figure 4. Mean daily course of (a) the net radiation (thick dotted line in the topmost figure), the slope and the valley wind components at several values of z/h; and (b) $\overline{u'w'}$ and $\overline{v'w'}$ at several values of z/h. For (a), positive (negative) values of thick lines indicate upslope (downslope) winds and positive (negative) values of thin dotted lines stand for a velocity component along the contour line in the up (down) valley direction.

maximum lies just above the canopy; with further increasing height wind speed decreases.

Reynolds stress $\overline{u'w'}$ is greatest just above the canopy. In the lower canopy and in the trunk space $\overline{u'w'}$ becomes very small and is mainly positive. The canopy hence acts as a sink for longitudinal momentum for the flow both above and beneath it. Another interesting feature is the lateral kinematic momentum flux $\overline{v'w'}$, which, after rotating the coordinate system into the mean wind, becomes zero on an infinite flat plane and negligibly small at near ideal sites (Kaimal and Finnigan, 1994). In situations where two wind systems of different (spatial and time) scale are interacting this can of course not be expected. Directional shear causes a lateral momentum transport that is in the same order at, or even larger than, the longitudinal one. In the trunk space where winds are essentially directed slope upwards negative daily $\overline{v'w'}$ values represent a momentum transport in the upvalley direction; $\overline{v'w'}$ decreases continuously with decreasing height. At night momentum fluxes are generally very small and of varying sign.

4.2. TURBULENCE PROFILES

In the 'family portrait', where common features of profiles of different canopies are depicted (e.g., Raupach, 1988), mainly neutral and near-neutral conditions are analysed. Therefore we show the neutral values of vertical profiles of turbulence statistics ± 1 standard deviation for comparison. The most frequently observed class, however, is that for weakly unstable daytime conditions. Additionally, unstable values from the morning transition time are given. In the following the abbreviation $\mathrm{CL}_{z=h}$ is used for a canopy layer at height $z = h$ and SL stands for surface layer. Reference neutral surface-layer values are taken from Panofsky (1984), whilst canopy layer values are taken from Raupach et al. (1996) and Finnigan (2000).

The neutral $\bar{u}/\bar{u}_{(h)}$ profile in Figure 5a is comparable to the profiles of the family portrait. The wind profile is inflected and gradients reach maximum values at $z = h$. Standard deviations are small, indicating that a good coupling exists between the different levels. There is a strong decrease of $\bar{u}/\bar{u}_{(h)}$ with descending height and minimum values are reached at the lowest level. This is not the case for both unstable and weakly unstable profiles. Even though the profiles are very similar in and above the canopy, they show primarily thermally induced wind speed maxima in the trunk space. During the morning transition the still dominating cold air drainage leads to maximum wind speeds at the lowest level and during the day buoyancy driven upslope winds lead to a maximum in the upper trunk space.

In the literature above-canopy flow is usually characterised by a constant momentum flux; within the canopy $\overline{u'w'}$ decreases rapidly. Here, as already mentioned, $\overline{u'w'}$ is greatest just above the canopy during daytime conditions and becomes very small and even mainly positive in the canopy layer whereas $\overline{v'w'}$ decreases continuously with decreasing height for all stability classes (Figures

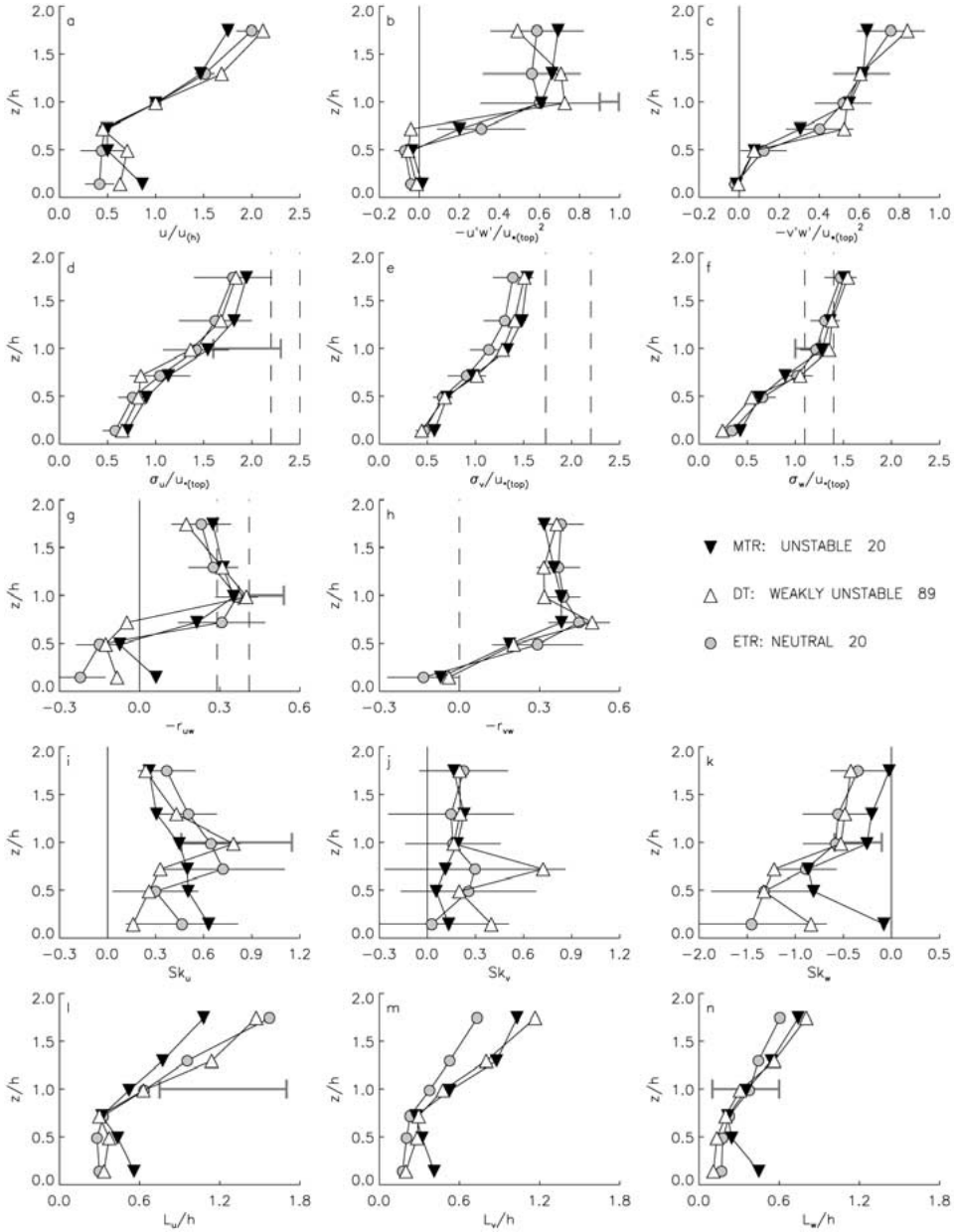

Figure 5. Normalised vertical profiles of (a) $u/u(h)$, (b) $-\overline{u'w'}/u^2_{*(\mathrm{top})}$, (c) $-\overline{v'w'}/u^2_{*(\mathrm{top})}$, (d), (e), (f) $\sigma_u/u_{*(\mathrm{top})}$, and, (g), (h) the correlation coefficients $-r_{uw}$, $-r_{vw}$, (i), (j), (k) skewnesses of u, v, w and (l), (m), (n) the length scales L_u/h, L_v/h and L_w/h respectively. Error bars (for reasons of clarity they are only given for neutral values) stand for ± 1 standard deviation. Dashed lines indicate ranges or values observed in the surface layer (Panofsky, 1984). Canopy-layer expectation ranges (Raupach et al., 1996) are given with grey horizontal lines in $z/h = 1$. Symbols show stability conditions and number of runs used in the respective profile.

5b,c). More information about momentum transport mechanisms can be gained by examining the joint probability distribution of the normalised velocity fluctuations (Figure 6). Above the canopy the probability for u', w' as well as v', w' to occur at the same time and in the same intensity is highest in the second quadrant. Momentum is thus most frequently transported by ejections, slow moving air masses that are transported upwards. Contributions of larger magnitude however arise from sweeps that transport high speed air downwards. For longitudinal momentum transport this ejection sweep dominance is not as distinctive as observed over other forests (e.g., Maitani and Shaw, 1990; Shaw et al., 1983), and is thus less organised. In the trunk space and during daytime in the upper canopy interactions are most frequent, resulting in a small but upward directed . Distributions of $v'w'$, however, become increasingly symmetric towards the ground indicating continuously smaller fluxes with decreasing height. Generally distributions at $z/h \leq 0.99$ show a stronger kurtosis, especially in the crown space where mainly small fluctuations of the second quadrant contribute to the flux and momentum transport is most intermittent. For $u'w'$ this is consistent with observations over other rough surfaces (e.g., Kruijt et al., 2000).

Figures 5d–f show the normalised standard deviations of the wind components. Positive deviations of σ_u/u_* from surface-layer scaling are often attributed to large-scale disturbances that scale with the height of the planetary boundary layer (e.g., De Bruin et al., 1993; Peltier et al., 1996). Here, however, fluctuations in the longitudinal direction are small even above the canopy compared to both SL and $\mathrm{CL}_{z=h}$ values (Figure 5d). As spectral analysis shows (Figure 7) there are few large-scale disturbances, possibly because large-scale eddies are topographically forced to remain stationary. σ_v/u_* values reach surface layer values well above the canopy; $\mathrm{CL}_{z=h}$ values were not found in literature for the lateral component. Neutral σ_w/u_* values above the canopy are slightly higher than SL values and reach SL values at $z = h$. Weak unstable and unstable above-canopy values lie in the range that one would expect in the surface layer; all second moments decrease rapidly in the canopy, which is in agreement with the 'family portrait'.

In forests over flat terrain the correlation coefficient of the longitudinal and vertical wind velocity components r_{uw} usually increases towards the rough surface and has a value of -0.5 at $\mathrm{CL}_{z=h}$. Figure 5g shows that r_{uw} increases towards the canopy, but there only a value close to those measured in a SL is observed. Contrary to both SL and CL where r_{vw} is close to zero, here r_{vw} values are significant for all but the lowest level. In the canopy all correlation coefficients decrease quickly and reach positive values for r_{uw}. Even though longitudinal momentum transport is not as effective as observed over other rough surfaces directional shear leads to the fact that more momentum is extracted from the mean flow than in both the SL and CL.

Longitudinal skewnesses in crown space are towards the lower end compared to those observed in the family portrait too (Figures 5i–k). Above the canopy however skewnesses do not drop to zero as rapidly as over forests in flat terrain. The positive u, v and the negative w third-order moments indicate that ejection sweep cycles are

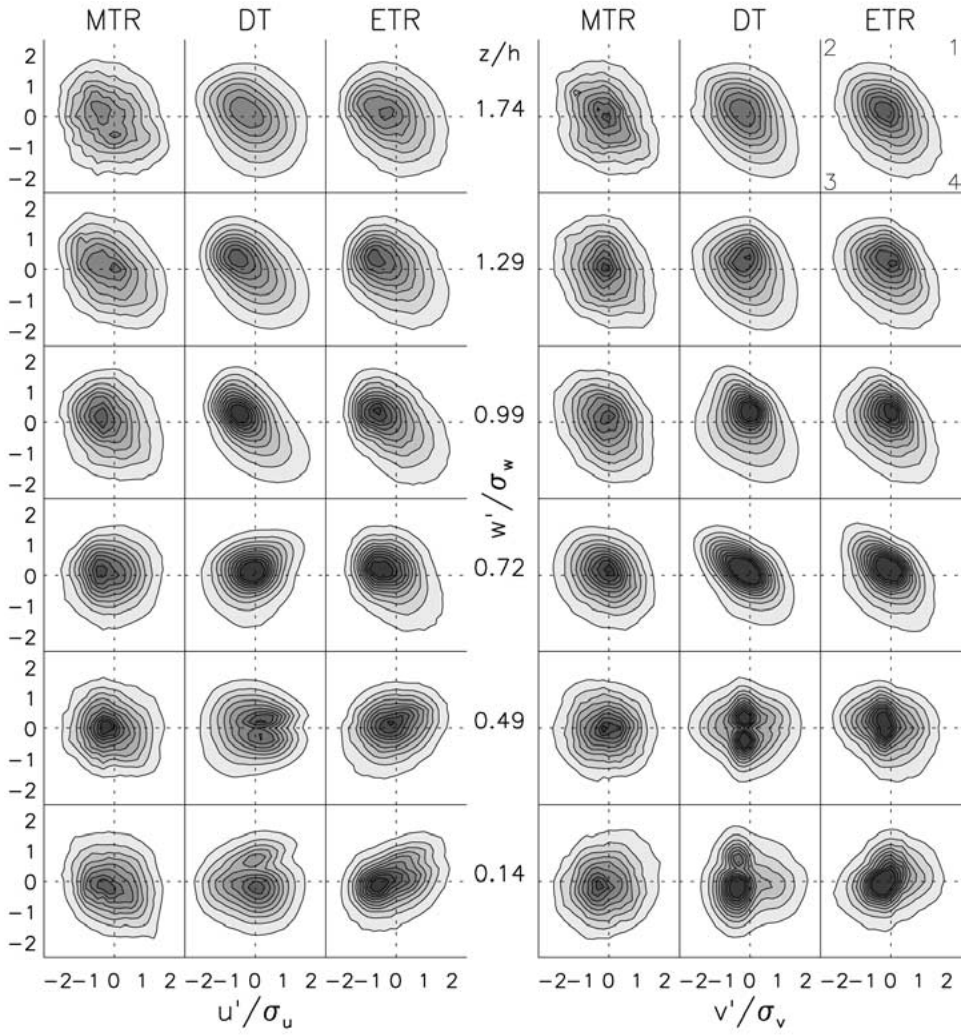

Figure 6. Joint probability distributions $P(u, w)$ and $P(v, w)$ of normalised fluctuations. Contour lines stand for 0.001 probability intervals. For the outermost contour $P = 0$. Definition of quadrants is given in the graph in the upper right corner.

important for momentum transport in the upper canopy as is confirmed by the joint probability density functions of the velocity fluctuations (Figure 6). But smaller CL correlation coefficients and skewnesses indicate that exchange mechanisms are less efficient and not as organised as over flat terrain.

According to Raupach et al. (1996) length scales L_u in the upper canopy are typically in the order of h. Here L_u/h is found to be towards the lower end compared to those observed in other forests (Figures 5l–n) but increases quickly above the crown space. $L_{w(h}$ is around $h/3$, which coincides with literature values.

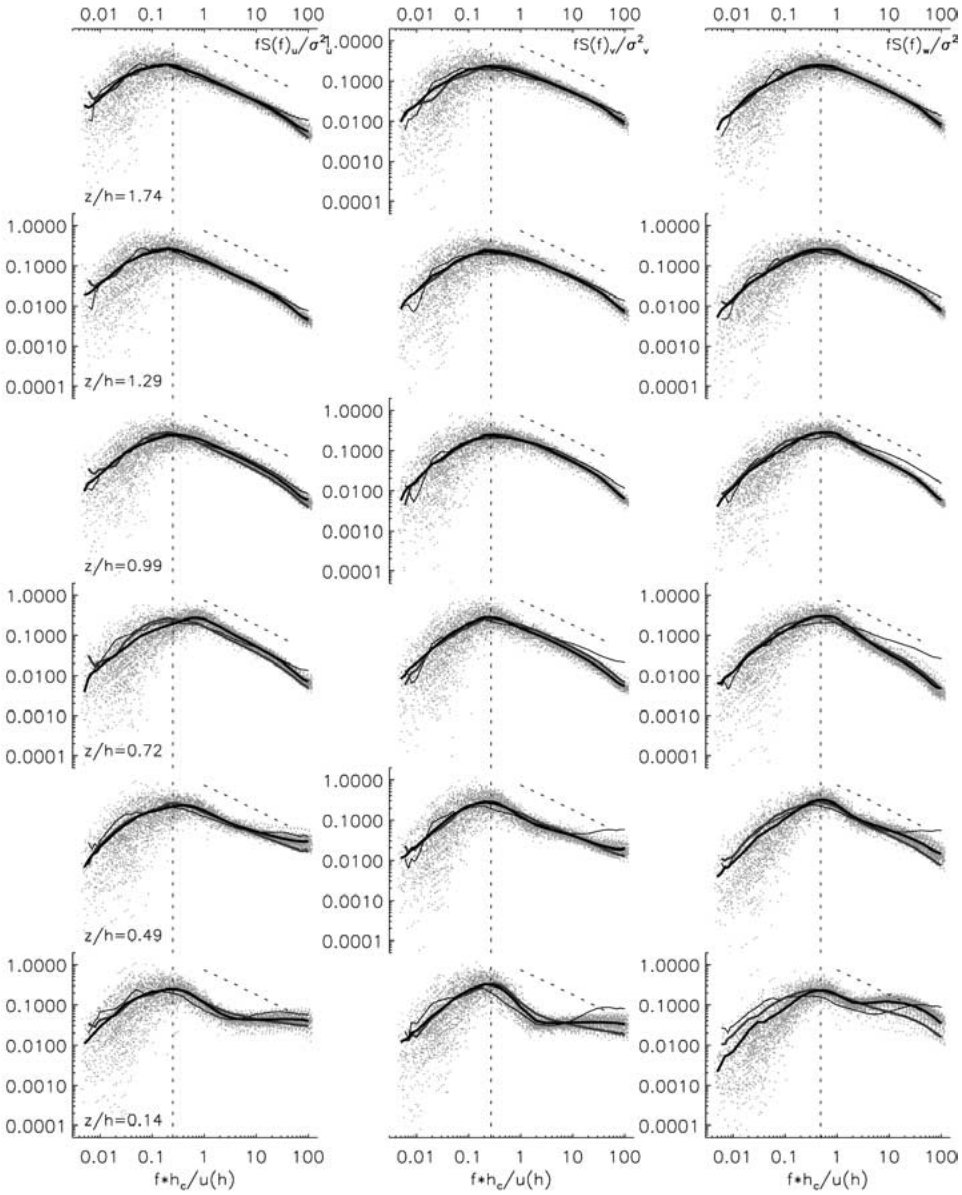

Figure 7. Normalised power spectra of all velocity components. Black thick, grey thick and black thin lines stand for weak unstable, unstable and neutral spectra respectively. Grey symbols indicate the scatter of weakly unstable spectra. Black dashed lines indicate $-2/3$ slope of inertial subrange. For easier orientation the vertical dashed line is given, indicating the peak frequency at $z/h = 0.99$ of weakly unstable conditions.

Raupach et al. (1996) suggested that the basic shear length scale in a canopy flow is $L_s = u_h/(\partial u/\partial z)_{z-h}$ and lies typically around $0.5h$ in moderately dense forests. From the mixing layer analogy they expected Λ_X, $(\partial u/\partial z)_{z=h}$ the x-distance between dominant eddies, to be in the range of 7 to 10 times L_s and found a mean value of 8.1 for all canopies they investigated. They further suggested that Λ_X is related to L_w by $\Lambda_X = 2\pi L_{w(h)}(u_c/u_{(h)})$, where u_c represents the convection velocity of eddies. Here L_s has been estimated from the measurements at z/h = 0.99 and the two neighbouring levels. For daytime conditions it lies at $0.46h$ and therefore very close to the values observed in other moderately dense forests. If $1.8u_{(h)}$ is used as an empirical value for u_c (e.g., Shaw et al., 1995), then Λ_X/h = 3.47 and thus Λ_X is 7.6 times L_s, which is in good agreement with the mixing layer analogy too. Further information on length scales can also be obtained by the maximum peak frequency $f_{\max}$ of spectra, which will be discussed below.

4.3. Spectral statistics

Figure 7 shows the normalised spectra of the wind velocity components. Several studies over flat terrain (e.g., Kaimal and Finnigan, 1994) have shown that, if the frequency axis is scaled with the mean canopy height h and the wind velocity (u_h), the position of peaks does not vary with height through the roughness sublayer (RS) to the mid canopy height.

Above the canopy, in the roughness sublayer, one has observed that energy is removed from the mean flow and injected into coherent eddies. In the canopy work is done against pressure drag and against the viscous component of canopy drag. Kinetic energy is then directly converted into fine scale wake turbulence and heat, (Kaimal and Finnigan, 1994). These processes extract energy from the mean flow and from eddies of all scales larger than the canopy elements. This continuous removal of energy from the eddy cascade leads to a violation of the assumptions leading to Kolmogorov's hypothesis.

The positions of the spectral peaks are given in Table 2. For the vertical velocity component the peaks lie in the range of literature values and they are fairly constant with height through the crown space. Relating the spectral peak frequency with Λ_X leads to $\Lambda_X/h = u_c/(f_{\max(w)}h) = 3.76$, a value that is in good agreement with the value evaluated using the integral length scale and therefore with the mixing layer analogy too. Lateral peak frequencies that have been measured in other forests are more variable than for the other velocity components. Here they lie in the indicated range of canopy data and they are fairly constant with height. This is not the case for the longitudinal component under weak unstable conditions. While at $z/h \geq 0.99$ the main energy contribution derives from eddies of similar size as observed in other studies, larger eddies seem to be suppressed in the crown space and peak frequencies are shifted to higher values. The reason for this is not clear. In the morning and evening transitions, however, the spectral peaks are fairly constant with height.

TABLE II

Scaled peak frequencies $f_{\max}$ for all velocity components and weak unstable (daytime) conditions. For comparison, literature values from Kaimal and Finnigan (1994) are indicated at the top of each column.

z/h	$f_{\max(u)}h/u_h$ 0.15 ± 0.05	$f_{\max(v)}h/u_h$ 0.10–0.35	$f_{\max(w)}h/u_h$ 0.45 ± 0.05
1.74	0.14	0.23	0.37
1.29	0.17	0.25	0.46
0.99	0.21	0.27	0.48
0.72	0.53	0.20	0.46
0.49	0.30	0.19	0.43
0.14	0.18	0.19	0.55

TABLE III

Inertial subrange slopes for all velocity components and weak unstable conditions calculated from normalised frequencies in the range of 1 to 10 Hz.

z/h	Slope (u)	Slope (v)	Slope (w)
1.74	−0.62	−0.53	−0.59
1.29	−0.64	−0.56	−0.61
0.99	−0.63	−0.58	−0.72
0.72	−0.69	−0.61	−0.89

There are remarkably few disturbances on the low frequency side of the spectra. While longitudinal and lateral spectra usually show quite large scatter that is caused by eddies larger than SL scales (e.g., Kaimal, 1978; Peltier et al., 1996), here spectral power falls off quickly on the low frequency side of the peak even under daytime conditions. Large-scale eddies might thus be topographically forced to remain stationary. Apart from the daily cycle a steady slope and valley wind system develops and there is a quite sharp separation between mean flow characteristics and turbulence.

Longitudinal power spectra are 'well behaved' in the sense that they follow the expected −2/3 slope in the inertial subrange closely over roughly two decades (Table III). Lateral power shows a smaller roll off at all measurement levels and vertical spectra have a smaller roll off above the canopy and a stronger than the −2/3 roll off from canopy top downwards. In general the canopy spectra show a

relative power deficit in the lower inertial subrange when approaching and descending through the canopy. This is most notable for spectra of the vertical wind component and may be attributable to wake and waving production processes that extract energy at larger scales and lead to a more pronounced importance of small-scale turbulence. In the trunk space, however, all spectra show a much steeper than $-2/3$ slope from the peak frequency until a normalized frequency $n \approx 1$, which corresponds roughly to a wavelength of 13 m, i.e., the canopy height. Additional energy is shifted to smaller wavelengths. It is unlikely that aliasing is the cause of this additional energy above the Nyquist frequency, since data collected with CSAT3 have been oversampled three times, which reduces aliasing effects. Vertical spectra especially support a source of smallest scale turbulence, which may be attributed to wake turbulence generation (Mazzoni, 1996; Kruijt et al., 2000).

5. Conclusions

The boundary layer of the forested slope we investigated shows an inflection point in the wind profile that is a characteristic feature of a canopy layer. Therefore many features of both canopy flow and mixing layers are observed in the present dataset. However larger scale thermally induced pressure fields lead to characteristic features, such as a change of wind direction with height associated with directional shear and lateral momentum transport, which are superimposed on the canopy flow.

In summary a comparison of velocity moments to the 'family portrait' leads to the following picture: (i) As in other forests the wind profile is inflected and maximum shear is located at canopy top; (ii) second-order moments decrease with height. Standard deviations of the longitudinal velocity component, however, are smaller than the canopy layer reference values at canopy height. Spectral analysis indicates that there are remarkably small low frequency disturbances. Large-scale eddies might be topographically forced to remain quasi stationary when the slope and valley wind system has developed; (iii) Even though the skewness of the longitudinal wind component in the crown space is towards the lower end compared to forests on flat terrain, the magnitudes of the skewnesses of all components in the crown space are still significant indicating that coherent structures are important for turbulent transport processes.

Acknowledgements

The Swiss National Science Foundation #21-55874.98 provided funding for this study. Thanks to Dr. N. Kalthoff from FZ Karlsruhe for the loan of several sonics.

References

Barry, R. G.: 1992, *Mountain Weather & Climate*, 2nd edn., Routledge, London and New York, 402 pp.

Christen, A., van Gorsel, E., Andretta, M., Calanca, P., Rotach, M. W., and Vogt, R.: 2000, 'Intercomparison of Ultrasonic Anemometers during the MAP-Riviera Project', in *Ninth Conference on Mountain Meteorology*, Aspen, CO, August 7–11, 2000, American Meteorological Society, 45 Beacon St., Boston, MA, pp. 130–131.

Christen, A., van Gorsel, E., Vogt, R., Andretta, M., and Rotach, M. W.: 2001, 'Ultrasonic Anemometer Instrumentation at Steep Slopes: Wind Tunnel Study – Field Intercomparison – Measurements', in *MAP Meeting Schliersee*, in MAP Newsletter 15, May 14–16, pp. 206–209.

De Bruin, H. A. R., Kohsiek, W., and van den Hurk, B. J. J. M.: 1993, 'A Verification of Some Methods to Determine the Fluxes of Momentum, Sensible Heat, and Water Vapour using Standard Deviation and Structure Parameter of Scalar Meteorological Quantities', *Boundary-Layer Meteorol.* **63**, 231–257.

Egger, J.: 1990, 'Thermally Forced Flows: Theory', in W. Blumen (ed.), *Atmospheric Processes over Complex Terrain, 23*, American Meteorological Society, Boston, MA, pp. 43–57.

Finnigan, J.: 2000, 'Turbulence in Plant Canopies', *Annu. Rev. Fluid Mech.* **32**, 519–571.

Finnigan, J. J. and Brunet, Y.: 1995, 'Turbulent Airflow in Forests on Flat and Hilly Terrain', in M. P. Coutts and J. Grace (eds.), *Wind and Trees*, Cambridge Universtiy Press, Cambridge, pp. 3–40.

Kaimal, J. C.: 1978, 'Horizontal Velocity Spectra in an Unstable Surface Layer', *J. Atmos. Sci.* **35**, 18–24.

Kaimal, J. C. and Finnigan, J. J.: 1994, *Atmospheric Boundary Layer Flows*, Oxford University Press, Oxford, 289 pp.

Kruijt, B., Malhi, Y., Lloyd, J., Nobre, A. D., Miranda, A. C., and Pereira, M. G. P.: 2000, 'Turbulence Statistics above and within Two Amazon Rain Forest Canopies', *Boundary-Layer Meteorol.* **94**, 297–331.

Maitani, T. and Shaw, R. H.: 1990, 'Joint Probability Analysis of Momentum and Heat Fluxes at a Deciduous Forest', *Boundary-Layer Meteorol.* **52**, 283–300.

Mazzoni, R.: 1996, *Turbulenzstruktur im gestörten Nachlauf einer künstlichen Oberflächenmodifikation. Ein Feldexperiment*, Ph.D. Dissertation, ETH Zürich, Zürich, 133 pp.

Panofsky, H. A. and Dutton, J. A.: 1984, *Atmospheric Turbulence – Models and Methods for Engineering Applications*, J. Wiley, New York, 397 pp.

Peltier, L. J., Wyngaard, J. C., Khanna, S., and Brasseur, J.: 1996, 'Spectra in the Unstable Surface Layer', *J. Atmos. Sci.* **53**, 49–61.

Rannik, Ü. and Vesala, T.: 1999, 'Autoregressive Filtering versus Linear Detrending in Estimation of Fluxes by the Eddy Covariance Method', *Boundary-Layer Meteorol.* **91**, 259–280.

Raupach, M. R.: 1988, 'Canopy Transport Processes', in W. L. Steffen and O. T. Denmead (eds.), *Flow and Transport in the Natural Environment: Advances and Applications*, Springer, Berlin, pp. 95–127.

Raupach, M. R. and Finnigan, J. J.: 1997, 'The Influence of Topography on Meteorological Variables and Surface-Atmosphere Interactions', *J. Hydrol.* **190**, 182–213.

Raupach, M. R. and Thom, A. S.: 1981, 'Turbulence in and above Plant Canopies', *Annu. Rev. Fluid Mech.* **13**, 97–129.

Raupach, M. R., Finnigan, J. J., and Brunet, Y.: 1996, 'Coherent Eddies and Turbulence in Vegetation Canopies: The Mixing-Layer Analogy', *Boundary-Layer Meteorol.* **78**, 351–382.

Rotach, M. W., Calanca, C., Vogt, R., Steyn, D. G., Graziani, G., and Gurtz, J.: 2000, 'The Turbulence Structure and Exchange Processes in an Alpine Valley: The MAP-Riviera Project', in *Ninth Conference on Mountain Meteorology*, Aspen, CO, August 7–11, American Meteorological Society, 45 Beacon St., Boston, MA, pp. 231–234.

Shaw, R. H., Brunet, Y., Finnigan, J. J., and Raupach, M. R.: 1995, 'A Wind Tunnel Study of Air Flow in Waving Wheat: Two Point Velocity Statistics', *Boundary-Layer Meteorol.* **76**, 349–376.

Shaw, R. H., Tavangar, J., and Ward, D. P.: 1983, 'Structure of the Reynolds Stress in a Canopy Layer', *J. Clim. Appl. Meteorol.* **22**, 1922–1931.

Vogt, R.: 1995, *Theorie, Technik und Analyse der experimentellen Flussbestimmung am Beispiel des Hartheimer Kiefernwaldes*, Ph.D. Dissertation, University of Basel, Basel, 101 pp.

Whiteman, C. D.: 1990, 'Observations of Thermally Developed Wind Systems in Mountinous Terrain', in W. Blumen (ed.), *Atmospheric Processes over Complex Terrain, 23*, American Meteorological Society, Boston, MA, pp. 5–42.

Whiteman, C. D. and Allwine, K. J.: 1989, 'Deep Valley Radiation and Surface Energy Budget Microclimates. Part I: Radiation', *J. Appl. Meteorol.* **28**, 414–426.

Wood, N.: 2000, 'Windflow over Complex Terrain: A Historical Perspective and the Prospect for Large-Eddy Modelling', *Boundary-Layer Meteorol.* **96**, 11–32.